LIMNOLOGY and OCEANOGRAPHY

Seasonal and spatial variability in surface pCO_2 and air–water CO_2 flux in the Chesapeake Bay

Baoshan Chen [ORCID],[1*] Wei-Jun Cai [ORCID],[1*] Jean R. Brodeur,[1] Najid Hussain [ORCID],[1] Jeremy M. Testa [ORCID],[2] Wenfei Ni,[3] Qian Li[1]

[1]School of Marine Science and Policy, University of Delaware, Newark, Delaware
[2]Chesapeake Biological Laboratory, University of Maryland Center for Environmental Science, Solomons, Maryland
[3]Horn Point Laboratory, University of Maryland Center for Environmental Science, Cambridge, Maryland

Abstract

Interactions between riverine inputs, internal cycling, and oceanic exchange result in dynamic variations in the partial pressure of carbon dioxide (pCO_2) in large estuaries. Here, we report the first bay-wide, annual-scale observations of surface pCO_2 and air–water CO_2 flux along the main stem of the Chesapeake Bay, revealing large annual variations in pCO_2 (43–3408 μatm) and a spatial-dependence of pCO_2 on internal and external drivers. The low salinity upper bay was a net source of CO_2 to the atmosphere (31.2 mmol m^{-2} d^{-1}) supported by inputs of CO_2-rich Susquehanna River water and the respiration of allochthonous organic matter, but part of this region was also characterized by low pCO_2 during spring and fall phytoplankton blooms. pCO_2 decreased downstream due to CO_2 ventilation supported by long water residence times, stratification, mixing with low pCO_2 water masses, and carbon removal by biological uptake. The mesohaline middle bay was a net CO_2 sink (−5.8 mmol m^{-2} d^{-1}) and the polyhaline lower bay was nearly in equilibrium with the atmosphere (1.0 mmol m^{-2} d^{-1}). Although the main stem of the bay was a weak CO_2 source ($3.7 \pm 3.3 \times 10^9$ mol C) during the dry hydrologic (calendar) year 2016, our observations showed higher river discharge could decrease CO_2 efflux. In contrast to many other estuaries worldwide that are strong sources of CO_2 to the atmosphere, the Chesapeake Bay and potentially other large estuaries are very weak CO_2 sources in dry years, and could even turn into a CO_2 sink in wet years.

Estuaries are important sites for understanding carbon cycling, due to their disproportionate contribution to air–water CO_2 fluxes. With only 0.3% of the global ocean surface area, estuaries release about 0.1–0.25 Pg C y^{-1} into the atmosphere, counterbalancing about 17% of the CO_2 uptake of the open oceans (Cai 2011; Chen et al. 2013). However, estimates of estuarine CO_2 flux still have large uncertainties due to a paucity of data coverage (e.g., limited research for low-latitude estuaries (Borges 2005) and in large estuaries and bay systems in the US mid-Atlantic coast (Joesoef et al. 2015)), as well as poor spatial and temporal coverage. Moreover, there are large uncertainties in estimating CO_2 flux through calculated partial pressure of carbon dioxide (pCO_2) when including discrete alkalinity observations, especially in low salinity waters, because of organic alkalinity and uncertainties in carbonic acid dissociation constants. Additionally, estuarine CO_2 fluxes exhibit high spatial heterogeneity as well as diurnal and seasonal variability. This variability tends to be the major source of bias in conclusions drawn from sporadic observations. To

better understand the contribution of estuaries to the global carbon cycle, frequent and long-term field investigations with sufficient spatial and temporal coverage and studies across estuarine types are clearly needed.

Estuaries receive large amounts of dissolved and particulate carbon from rivers, which undergo significant transformation before being transferred to the adjacent coastal seas. These complex biogeochemical processes determine the magnitude and direction of air–water CO_2 flux. Most estuaries are characterized by oversaturated surface pCO_2 (Chen and Borges 2009; Cai 2011) from degraded allochthonous organic matter, with community respiration exceeding gross primary production. Indeed, most estuaries are net heterotrophic and net sources of CO_2 to the atmosphere (Gattuso et al. 1998; Battin et al. 2008). However, other factors, including calcium carbonate ($CaCO_3$) formation/dissolution, exchange of water inputs from adjacent aquatic systems with different pCO_2 signals, water residence time, and stratification can modulate air–water CO_2 flux and even drive the system to absorb CO_2 from the atmosphere (Borges et al. 2006). In particular, permanent or seasonal water stratification plays an important role in modifying surface pCO_2 by decoupling organic matter production

*Correspondence: bschen@udel.edu; wcai@udel.edu

in surface waters from respiration below the pycnocline, where respired CO_2 does not readily exchange with the atmosphere. The result is that production in surface waters decreases pCO_2 and can drive the surface mixed layer to be a CO_2 sink, despite generating a subsurface large respiration signal (Kone et al. 2009). Estuary size and type also influence the CO_2 flux. Smaller estuaries show more significant heterotrophy than larger estuaries (Caffrey 2004). Large river-dominated estuaries and their plumes have been extensively studied (e.g., Amazon River (Cooley et al. 2007), Mississippi River (Huang et al. 2015), and Changjiang River (Zhai et al. 2007)), however, few studies have been conducted in large bays with moderate river input and a long water residence time. Limited recent research has shown that pCO_2 values in these ocean-dominated, large estuaries are much lower than river-dominated small estuaries (Joesoef et al. 2015; Dinauer and Mucci 2017).

The Chesapeake Bay is the largest estuary in the United States with a length of about 300 km, a width of 8–48 km, an average depth of 8 m, and a main stem trench up to 50 m (Cerco and Cole 1993). It is a partially mixed and microtidal estuary with two-layer circulation. Spatially, it is characterized by interactions between a river-dominated upper bay and an ocean-dominated lower bay, with a long, average water residence time of 180 d (Du and Shen 2016). The Chesapeake Bay is undergoing increasing pressure from nearby population growth (Orth et al. 2017), and has been characterized by severe long-term eutrophication due to riverine nutrient inputs (Boesch et al. 2001; Kemp et al. 2005). These nutrient inputs stimulate the production of organic matter, which during strong summer stratification sinks below the pycnocline and is respired where ventilation is prevented, resulting in summer hypoxia and anoxia in the deep trench (Officer et al. 1984; Hagy et al. 2004). Although the Chesapeake Bay has received wide research attention, until recently only limited studies on the inorganic carbon dynamics have been conducted, including early research in some tributaries in the lower bay (Wong 1979; Raymond et al. 2000). Recent studies of the CO_2 system include investigations at one upper bay station in summer 2013 (Cai et al. 2017), the bay-wide seasonal and spatial distribution of DIC, TA, and pH (Brodeur et al. 2019), a model simulation of pCO_2 in the bay (Shen et al. 2019), and a study of seasonal mass balance of DIC in the middle and lower bay (Friedman et al. 2020). So far, no comprehensive annual CO_2 flux of the Chesapeake Bay has been reported, nor included in the global estuarine CO_2 flux synthesis (Cai 2011; Chen et al. 2013; Laruelle et al. 2015). Therefore, there is a need for comprehensive understanding of the spatial and temporal distribution patterns of surface pCO_2 for reporting annual CO_2 flux and determining the CO_2 source/sink status of the Chesapeake Bay.

In this work, we aimed to define the distribution patterns and controlling mechanisms of surface CO_2 in the Chesapeake Bay. We first reported high resolution, underway measurements of surface pCO_2 and discrete samples of the carbonate system over 10 months in 2016 and one winter cruise in 2019. Then, we delineated the processes influencing pCO_2 distribution and variability, by studying their variability and magnitude from the bay head to bay mouth. Finally, we determined the magnitude of CO_2 flux and discussed the uncertainties in the estimates resulting from differences between underway and discrete sampling strategies, spatial variability, diel variation, and hydrological conditions.

Methods

Study site and cruise information

The Chesapeake Bay was divided into three subregions following the approach in Kemp et al. (1997), including an upper bay (> 39.0°N, 11% of total area), a middle bay (37.9–39.0°N, 36% of total area), and a lower bay (< 37.9°N, 53% of total area) (Fig. 1). We conducted four bay-wide cruises in the Chesapeake Bay on R/V *Rachel Carson* on 04–06 May, 06–10 June, 08–12 August, and 10–13 October 2016, and one bay-wide cruise on a commercial boat on 21–22 February 2019, hereafter referred to as "*Carson* cruises." In addition, we conducted six cruises on the R/V *Randall T. Kerhin* on 14–16 March, 12–13 April, 11–13 July, 19–21 September, 14–15 November,
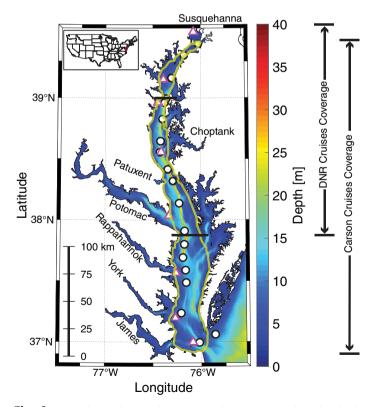

Fig. 1. Map of the Chesapeake Bay, including water depth (color shading), discrete hydrographic stations (circles), buoy stations (triangles), the boundary of the bay main stem for the air-sea CO_2 flux estimate (yellow line), and the boundaries separating the upper bay (> 39°N), middle bay (37.9–39.0°N), and lower bay (< 37.9°N) (black lines).

and 12–14 December 2016, which are subsequently referred to as "*DNR* cruises." The hydrographic sampling stations in the *Carson* cruises were mostly selected from the Maryland and Virginia water quality monitoring stations for historical comparison. Both underway monitoring and discrete sampling were conducted spanning from the near-zero salinity estuary of the Susquehanna River to the mouth of the bay, mainly along the central axis. The only exception is that the May *Carson* cruise only covered the upper, middle, and northernmost part of the lower bay, omitting the rest of the lower bay stations. The *DNR* cruises included the Maryland portion of the water quality monitoring stations, with the southernmost point reaching the mouth of the Potomac River. No underway monitoring was conducted on the *DNR* cruises.

Discrete and underway measurements

At each station, we collected discrete surface samples (~ 0.5 m below surface) for dissolved inorganic carbon (DIC) and pH during all cruises, and sampled dissolved oxygen (DO) as well during the *Carson* cruises. For the *DNR* and most of the *Carson* cruises, we used an in situ profile pumping system equipped with a YSI 6600 (Xylem) to take samples and record in situ temperature and salinity. On the February 2019 *Carson* cruise, we collected samples from an underway flow-through system of the boat. Water temperature and salinity were recorded by a thermosalinograph (SBE45, Sea-Bird Scientific) inside an underway partial pressure of carbon dioxide (pCO₂) system (AS-P2, Apollo SciTech) in the onboard lab. The measured temperature was used as the in situ surface water temperature, because surface water was pumped through a short standpipe directly to the lab in seconds and the temperature difference between in situ surface water (~ 0.5 m, with a NIST traceable thermometer) and the pCO₂ system was negligible (< 0.1°C).

DIC was sampled in 250 mL borosilicate glass bottles and preserved with 50 μL of saturated HgCl₂ solution. pH was collected in 120 mL soda lime glass bottles and not preserved. DIC was analyzed using an automated DIC analyzer (AS-C3, Apollo SciTech), with a precision of 0.1% and an accuracy of ± 2 μmol kg⁻¹. pH was measured on the NBS scale at 25°C using an Orion ROSS Ultra pH electrode (8102BNUWP, Thermo Scientific) and calibrated against three NBS pH buffers (pH = 4.01, 7.00, and 10.01), with a precision of ± 0.003 pH units. More sampling and measurement details were shown in Brodeur et al. (2019). DO samples were collected in 60 mL BOD bottles and stored in the dark with a water seal to prevent gas exchange, which were spectrophotometrically determined within 48 h by a modified Winkler method (Pai et al. 1993). In addition, we measured underway surface pCO₂ and DO during the *Carson* cruises using the underway pCO₂ system. Surface pCO₂ was measured approximately every 1.5 min using a shower head type equilibrator. The pCO₂ system was calibrated every 6–12 h against four compressed CO₂ gas standards (150.62, 404.72, 992.54, and 1984.82 ppm CO₂

in air), which are traceable to the World Meteorological Organization (WMO) scale. Atmospheric pCO₂ was measured every 3–6 h using the same CO₂ system. The precision of underway pCO₂ measurements is 0.1 μatm and the overall accuracy is estimated at 2 μatm. DO was measured by an Aanderaa optical oxygen optode 4531 (Xylem). The DO optode has a resolution of < 1 μM and its accuracy was calibrated against discrete DO samples.

Mooring data of the Chesapeake Bay interpretive buoy system

We obtained monthly and annual mean wind speed and surface water temperature in the subregions and over the entire bay from the mooring data of the Chesapeake Bay Interpretive Buoy System (https://buoybay.noaa.gov/observations/data-download). The eight buoys along the main stem were included to derive these values (Fig. 1). In some months, there was limited buoy data to calculate the monthly average, due to service problems. To address this, we first averaged available monthly data for each buoy and then averaged other buoy data collected in the same subregion. For wind speed, we corrected observed wind speed (3 m) to a 10 m height using the proposed equation in the Shore Protection Manual (1984). For surface temperature, we calculated the seasonal mean surface temperature for the upper, middle, and lower bay and then averaged them to get a bay-wide annual mean surface temperature of 17 ± 0.1°C in 2016.

Susquehanna River end-member properties

We monitored the Susquehanna River end-member temperature, salinity, DIC, and pH values monthly at the Conowingo Dam (USGS site #01578310) in 2016, except in March and April, when we collected samples at the nearby Havre de Grace station. Monthly Chlorophyll a (Chl a) for the Susquehanna River was measured at the river mouth (Sta. CB1.0) by the Chesapeake Bay Program (www.chesapeakebay.net). Monthly mean river discharge was from the Conowingo Dam (https://waterdata.usgs.gov/md/nwis/uv?site_no=01578310).

Calculation of pCO₂ in surface mixed layer

Since there was no direct pCO₂ measurement during the *DNR* cruises, we calculated surface pCO₂ from the discrete surface DIC and pH measurements, using the Excel version of CO2SYS (Pierrot et al. 2006), with carbonic acid dissociation constants K_1 and K_2 from Millero et al. (2006), K_{HSO_4} from Dickson (1990), and total boron from Uppström (1974), according to the recommendations in previous studies (Millero et al. 2006; Orr et al. 2015). We used DIC and pH, rather than TA, to calculate pCO₂ to avoid the uncertainties of calculation associated with organic alkalinity in estuarine waters (Cai et al. 1998), because CO2SYS neglects the contribution of organic alkalinity.

To evaluate the difference between calculated and underway measured pCO₂ values, we collected some discrete underway

DIC and pH samples in waters with salinity ≥ 5. Underway $p\text{CO}_2$ measurements were systematically higher than calculated values, with mean differences of 33 μatm ($n = 3$, mean salinity = 5) in the upper bay, 16 μatm ($n = 26$, mean salinity = 10) in the middle bay, and 15 μatm ($n = 31$, mean salinity = 16) in the lower bay. These differences in the middle and lower bay are on the same level as in temperate oceans (Wanninkhof et al. 1999). The relatively larger discrepancies in the upper bay are associated with the larger uncertainties of the carbonic acid dissociation constants at low salinities and likely sampling lag among these carbonate parameters in this dynamic environment (~ 2 min sampling interval for $p\text{CO}_2$). Given low salinity river water is limited to a small area of the upper bay, and the discrepancy in $p\text{CO}_2$ was relatively small when compared with riverine $p\text{CO}_2$ of up to 2000 μatm, the discrepancy in calculated $p\text{CO}_2$ only contributes to 0.7% of the CO_2 flux in the upper. Therefore, the uncertainties in calculated $p\text{CO}_2$ are acceptable.

Air–water CO₂ flux calculation

CO_2 flux (F) in units of mmol CO_2 m^{-2} d^{-1} was calculated following Wanninkhof (2014) (Eq. 1):

$$F = k \times K_0 \times \left(p\text{CO}_{2(\text{water})} - p\text{CO}_{2(\text{air})} \right) \tag{1}$$

where k is the widely used gas transfer velocity of CO_2 gas in cm h^{-1}, K_0 is the solubility of CO_2 at a specific temperature and salinity in mol kg^{-1} atm^{-1}, and $p\text{CO}_{2(\text{water})}$ and $p\text{CO}_{2(\text{air})}$ are in situ $p\text{CO}_2$ values in surface waters and cruise-averaged atmospheric $p\text{CO}_2$ values in μatm. Monthly mean wind speeds at 10 m height used to calculate CO_2 flux were from the Chesapeake Bay Interpretive Buoy System buoy data. A positive flux indicates that surface waters are degassing CO_2 into the atmosphere.

To get an accurate area-averaged CO_2 flux, we divided the Chesapeake Bay into fine latitudinal segments. Each segment has a width of the main stem of the bay and a north–south resolution of 0.01°. We averaged all CO_2 flux measurements within each segment to get a representative flux, which was multiplied with the segment area to get a CO_2 flux of the segment. The area-averaged CO_2 flux was calculated by normalizing the sum of all CO_2 fluxes to the total areas of segments with data. We then evaluated area-averaged CO_2 fluxes (F_A) for the upper, middle, and lower bay, and the entire bay using Eq. 2

$$F_A = \frac{\sum F_x \times A_x}{\sum A_x} \tag{2}$$

where F_x is the average of all CO_2 flux measurements within each segment and A_x is the corresponding sectional surface area. The uncertainty of CO_2 flux was estimated from the SD of the means for wind speed and the uncertainty of $p\text{CO}_2$ measurements using error propagation method.

Model-generated air–water CO₂ flux in the lower bay

To get a representative annual CO_2 flux in 2016, we improved the estimate of annual CO_2 flux by incorporating model-generated seasonally averaged CO_2 flux for 2016 from Shen et al. (2019). The model-generated CO_2 fluxes were used to compare with that in February 2019 and fill in data gap in the lower bay during the spring and winter of 2016. Generally, the model-generated seasonal trend of CO_2 fluxes agreed with the field observations, while model estimates had large uncertainties and the differences between model-generated seasonal mean and field observations were large (− 10 to 21 mmol m^{-2} d^{-1}) in the upper and middle bay. However, the model reproduced the CO_2 flux well in the lower bay (− 2 to 7 mmol m^{-2} d^{-1}). In this case, we used model-generated lower bay CO_2 fluxes of − 2.7 ± 9.0 mmol m^{-2} d^{-1} for winter, as well as − 1.5 ± 5.3 mmol m^{-2} d^{-1} for spring.

Simulation of surface pCO₂ levels in the lower bay

To study the potential difference in CO_2 flux between dry and wet months, we simply simulated surface $p\text{CO}_2$ variation from late fall to early spring in the lower bay under interactions among air–water gas exchange, surface water temperature change, and biological removal of inorganic carbon from the surface mixed layer. For the lower bay, a simplified simulation is a reasonable approach due to several months water residence time, low surface nutrient concentration, and relatively uniform surface $p\text{CO}_2$.

In the simulation, we used field measurements of carbonate parameters in the lower bay in October 2016 as the initial values, as well as mean atmospheric $p\text{CO}_2$, wind speed, surface mixed layer depth, biological DIC removal rate in surface mixed layer estimated from Kemp et al. (1997), and surface temperature. During each iterative calculation with a time step of 1 h, we first calculated the air–water CO_2 flux. This amount of CO_2 was added to the DIC inventory in the surface mixed layer, and biological DIC removal was subtracted. Then, we calculated a new surface $p\text{CO}_2$ using this biogeochemically modulated DIC and surface temperature at the time of the next iteration. The newly calculated $p\text{CO}_2$ was used for the next iterative calculation of air–water gas exchange.

Relationship of pCO₂ and DO variations

To explain biological modulation of surface $p\text{CO}_2$, we adopted the relationship between the high-resolution underway measurements of saturation states of $p\text{CO}_2$ and DO, i.e., $p\text{CO}_2$% and DO% respectively, with respect to the atmosphere. $p\text{CO}_2$% and DO% were calculated using Eqs. 3 and 4.

$$p\text{CO}_2\% = p\text{CO}_{2(\text{water})} \div p\text{CO}_{2(\text{air})} \times 100\% \tag{3}$$

$$\text{DO}\% = \text{DO}_{(\text{water})} \div \text{DO}_{(\text{saturated})} \times 100\% \tag{4}$$

where subscript (water) denotes in situ measurements. pCO_2 (air) is cruise-averaged atmospheric pCO_2 (μatm). $DO_{(saturated)}$ is saturated DO concentration (μmol kg^{-1}) in surface waters calculated from in situ water temperature and salinity.

Results

Spatial and temporal distribution of surface water pCO_2

Underway pCO_2 (*Carson* cruises) and pCO_2 calculated from discrete DIC and pH (*DNR* cruises) of each cruise is shown in Fig. 2 and monthly ranges and average pCO_2 values are summarized in

Table 1. The annual surface pCO_2 varied widely from 43 to 3408 μatm with a mean of 493 ± 304 μatm. Corresponding, annual atmospheric pCO_2 ranged from 389 to 423 μatm, with a mean of 403 ± 13 μatm. This significant annual variation in surface water pCO_2 corresponded to a large temperature range of 4–31°C and a salinity range of 0–31.

Spatially, surface pCO_2 generally decreased from the Susquehanna River towards the bay mouth, with an annual average of 901 ± 479 μatm in the upper bay, 416 ± 167 μatm in the middle bay, and 392 ± 98 μatm in the lower bay. Temporally, bay-wide (*Carson* cruises) surface pCO_2 was lower in cold
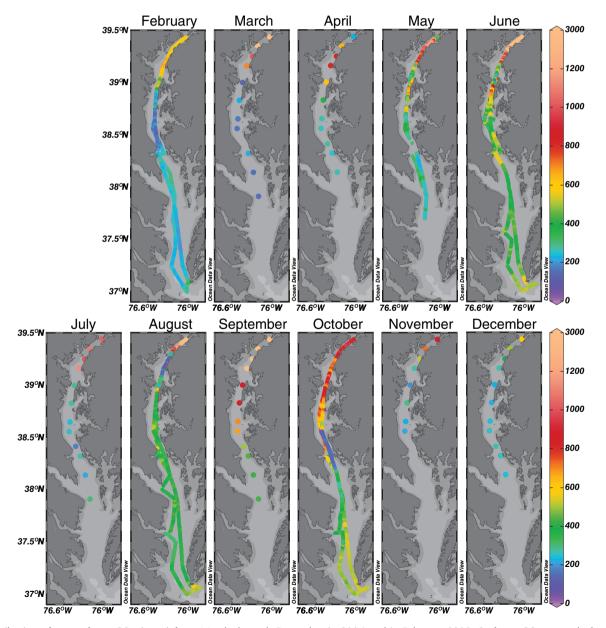

Fig. 2. Distribution of sea surface pCO_2 (μatm) from March through December in 2016 and in February 2019. Surface pCO_2 was calculated from discrete DIC and pH samples in March, April, July, and September, November, and December 2016 (*DNR* cruises). Surface pCO_2 was observed via continuous underway sampling in May, June, August, and October 2016 and in February 2019 (*Carson* cruises). The *DNR* cruises only covered the upper and middle bay, while the *Carson* cruises covered the whole bay.

Table 1. Mean ± SD and range of surface pCO$_2$ and monthly mean Susquehanna River discharge.

| Year | Month | pCO$_2$ (μatm) | | | | | | | | Susquehanna River discharge (m^3/s)[†] |
| | | Upper bay | | Middle bay | | Lower bay | | Whole study area[*] | | Monthly mean |
		Mean ± SD	Range	Mean ± SD	Range	Mean ± SD	Range	Mean ± SD	Range	
2016	Jan	N/A	N/A	N/A	N/A	N/A	N/A	N/A	N/A	1290
2019	Feb	595 ± 62	411–704	252 ± 77	103–563	246 ± 30	197–349	316 ± 149	103–704	2167
2016	Mar	1906 ± 1150	698–3408	173 ± 35	127–226	N/A	N/A	895 ± 1131	127–3408	1251
2016	Apr	642 ± 242	230–821	329 ± 136	247–626	N/A	N/A	459 ± 239	230–821	952
2016	May	977 ± 315	262–1437	350 ± 94	218–737	282 ± 37	244–416	551 ± 363	218–1437	1041
2016	Jun	1255 ± 569	104–2065	415 ± 121	202–870	438 ± 57	343–576	538 ± 366	104–2065	420
2016	Jul	1145 ± 159	1006–1410	254 ± 43	176–306	N/A	N/A	597 ± 461	176–1410	211
2016	Aug	782 ± 677	43–2565	431 ± 99	232–904	399 ± 60	300–588	468 ± 289	43–2565	288
2016	Sep	1907 ± 242	1566–2213	617 ± 194	424–893	N/A	N/A	1113 ± 684	424–2213	162
2016	Oct	869 ± 102	649–1109	620 ± 158[‡] (200 ± 84)[§]	368–1033[‡] (107–407)[§]	506 ± 32[‡] (383 ± 43)[§]	380–566[‡] (293–526)[§]	638 ± 117[‡] (285 ± 114)[§]	368–1109[‡] (107–526)[§]	384
2016	Nov	703 ± 316	297–1097	234 ± 44	193–296	N/A	N/A	495 ± 335	193–1097	390
2016	Dec	424 ± 120	275–584	246 ± 19	219–271	N/A	N/A	320 ± 118	219–584	855
Annual		901 ± 479	43–3408	416 ± 167	103–1033	392 ± 98	197–588	493 ± 304	43–3408	

*Surface pCO$_2$ data are available over the whole bay in the February, May, June, August, and October cruises, while they are available only for the upper and middle bay in March, April, July, September, November, and December.
†Monthly mean river discharge of Susquehanna River. Data downloaded from https://waterdata.usgs.gov/usa/nwis/uv?01578310.
‡Surface pCO$_2$ data of pre-bloom observations in October 2016, which represents normal pCO$_2$ distribution in late fall.
§Surface pCO$_2$ data of a bloom event trigger by a hurricane in October 2016.

months and higher in warmer months, with the lowest average pCO_2 in February (316 ± 149 μatm) and the highest pCO_2 in October (638 ± 117 μatm). Exceptions were observed under the modulation by a series of contrasting biological production and respiration states. Blooms resulted in large areas of low pCO_2 in the lower portion of the upper bay (August), the upper portion of the middle bay (February and June), and from the middle bay to the mid-reach of the lower bay (October) (Fig. 2). Moreover, blooms also resulted in a lower bay-wide average surface pCO_2 of 468 ± 289 μatm in August than months before and after.

Surface pCO_2 and npCO_2 vs. latitude

Surface water pCO_2 is plotted against latitude in Fig. 3a (*Carson* cruises) and Fig. 3b (*DNR* cruises). Surface pCO_2 normalized to the annual mean surface temperature of $17°C$ (npCO_2) is plotted in the same way in Fig. 3c,d. Given that pCO_2 in water increases by about 4.23% with a $1°C$ increase in temperature (Takahashi et al. 1993), the annual temperature cycle can increase bay-wide mean surface pCO_2 from 316 μatm in February to 990 μatm in August, accounting for 29% of the annual pCO_2 range. In this sense, large annual variations in water temperature could contribute to pronounced
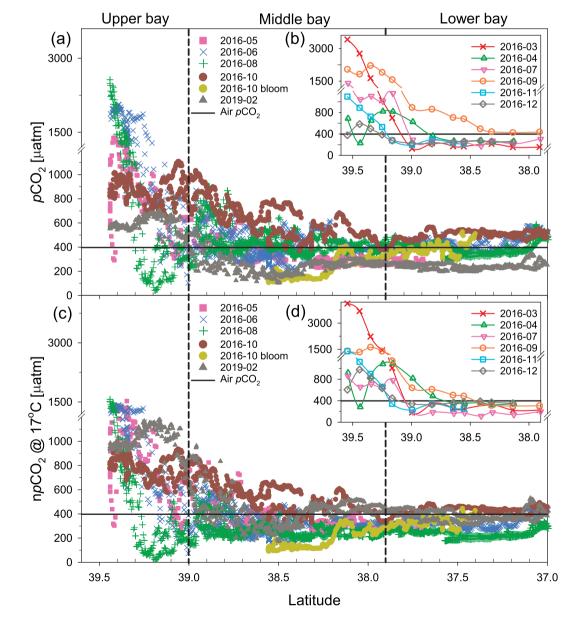

Fig. 3. Distributions of surface pCO_2 and temperature normalized pCO_2 (npCO_2) against latitude. Surface npCO_2 indicates pCO_2 values normalized to the annual mean surface temperature of $17°C$. The black vertical dashed lines are the boundaries of the upper, middle, and lower bay at $39.0°N$ and $37.9°N$. The black horizontal solid line indicates the annual mean atmospheric pCO_2 level. **(a)** and **(c)** for the *Carson* cruises cover the whole bay while inserted **(b)** and **(d)** for the *DNR* cruises only cover the upper and middle bay.

changes in pCO_2. Given $npCO_2$ removes the thermal influence on pCO_2, same $npCO_2$ over seasons suggests that temperature change dominates pCO_2 variation and the non-thermal processes, including physical mixing, air–water gas exchange, biological production/respiration, and chemical reactions, are weak or their effects counterbalance each other.

Surface pCO_2 decreased seaward, along with complex seasonal variations, with a large gradient in the early spring and summer (Fig. 3a,b). Regionally, the upper bay had the maximum pCO_2 gradient, as the Susquehanna River water had high pCO_2 year-round. Although the upper bay was supersaturated in pCO_2 at most times, undersaturated pCO_2 with respect to the atmosphere was observed slightly downstream of the Susquehanna River mouth (~ 39.4°N) in April (Fig. 3b) and May (Fig. 3a) and in the lower-reach of the upper bay in August (~ 39.2°N) (Fig. 3a). Under the influence of high pCO_2 riverine input (Fig. 3b) and high temperature in summer, there were two seasonal pCO_2 peaks observed in March (3408 μatm) and August (2565 μatm). However, due to the contribution of seasonal biological blooms, regionally average surface pCO_2 was lower in August (782 ± 667 μatm), as well as in April (642 ± 242 μatm) and May (977 ± 315 μatm), than months before and after. In addition, surface pCO_2 decreased from October (869 ± 102 μatm) to December (424 ± 120 μatm) until high river discharge brought high pCO_2 into the bay in the following spring.

The middle bay, serving as a transition zone to the low pCO_2 lower bay, had a weaker pCO_2 gradient than the upper bay. It also showed dynamic seasonal fluctuation between CO_2 sink and source status. Surface pCO_2 was undersaturated in most months except nearly equilibrated with the atmosphere in June (415 ± 121 μatm) and August (431 ± 99 μatm) and oversaturated in September (617 ± 194 μatm) and October (620 ± 158 μatm). For other months with undersaturated pCO_2, the pCO_2 in February and March reflected winter hydrographic patterns that the oversaturated spring riverine pCO_2 had not yet reached the middle bay when compared with that in April (247–626 μatm). Moreover, surface $npCO_2$ in April and May was at the same level while higher than in March (Fig. 3c,d), supporting carbon input into the middle bay from March to April and indicating the temperature dominance on pCO_2 variation from April to May. Similarly, lower $npCO_2$ in November and December than in October suggests carbon removal from the middle bay.

The lower bay pCO_2 had spatially invariant distribution and small seasonal variations, with undersaturation in February (246 ± 30 μatm) and May (282 ± 37 μatm), equilibrium in June (438 ± 57 μatm) and August (399 ± 60 μatm), and supersaturation in October (506 ± 32 μatm). Additionally, surface pCO_2 has a fast response to bloom events. In October, surface pCO_2 dropped by up to 100 μam in the middle and lower bay in response to a hurricane triggered bloom within 2 d.

Surface pCO_2 and $npCO_2$ vs. salinity

To study pCO_2 distribution patterns during mixing between riverine and oceanic water, surface pCO_2 and $npCO_2$ are plotted

against salinity in Fig. 4a,b and Fig. 4c,d, respectively. Based on the hydrographic features and pCO_2 variations, we divided the study area into 3 subregions: salinity 0–3, 3–12, and 12–33. Generally, the lowest salinity region was confined to the upper reach of the upper bay, the mid-salinity region covered areas of the lower-reach of the upper bay and most areas of the middle bay, and the highest salinity region occupied the lower-reach of the middle bay and the lower bay.

Salinities at which pCO_2 changed drastically varied seasonally (Fig. 4). Pronounced pCO_2 variations were observed in the upper bay (Fig. 3), following the changes of the Susquehanna River discharge which peaked in February and reached a minimum from July to September, with the lowest discharge in September (Table 1). This pattern indicates that Susquehanna River discharge was a major contributor to the large pCO_2 variations in the bay. In the salinity range of 0–3, the most variable pCO_2 values were observed at salinities close to 0, with both undersaturated $npCO_2$ and pCO_2 observed in April and May and oversaturated values observed in other months (Fig. 4). By comparison, estuarine turbidity maximum centered on average where salinity of 1 isohaline meets the bottom (Boynton et al. 1997). Invariant $npCO_2$ (~ 1500 μatm at ~ 39.4°N) clustered around the center of the estuarine turbidity maximum from May to September, showing that the increasing pCO_2 was dominated by temperature increase. It also indicates potential unifying regulation of pCO_2 in the estuarine turbidity maximum. In the salinity range of 3–12, pCO_2 decreased rapidly with increasing salinity, except in September and October, during which pCO_2 and $npCO_2$ were relatively uniform over the salinity range. In the salinity range of 12–33, surface pCO_2 had small variations over the year, except that pCO_2 varied up to 900 μatm at a narrow salinity range of 17–19 in September and October.

Although monthly river discharge and riverine pCO_2 input into the bay varied largely (Table 1 and Fig. 4), salinities at which surface pCO_2 decreased drastically and reached relatively invariant pCO_2 values were similar in some consecutive months: ~ 6 (February and March), ~ 12 (April–August, November, and December), and ~ 17 (September and October). This suggests a time lag in the response of salinity and pCO_2 to discharge variations. Additionally, the fact that pCO_2 decreased drastically at a similar salinity in some consecutive months might underscore the influence of long water residence times and an interaction between high pCO_2 riverine and low pCO_2 oceanic water masses. The largest vertical pCO_2 gradient observed at a surface salinity of ~ 17 in September and October suggests that high salinity and CO_2-rich subsurface water was brought to the surface due to the fall seasonal erosion of stratification. The mixing is evident in the high salinity, when it was only ~ 12 in the month before and after.

Air–water CO_2 fluxes

Lower bay air–water CO_2 influx in February 2019 (− 14.2 ± 1.5 mmol m^{-2} d^{-1}) (Table 2) was significantly larger
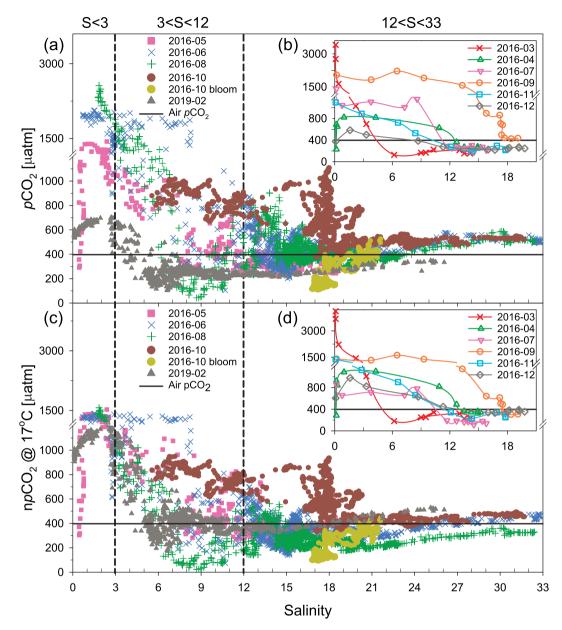
Fig. 4. Distributions of surface pCO_2 and temperature normalized pCO_2 ($npCO_2$) against salinity. Surface $npCO_2$ indicates pCO_2 values normalized to the annual mean surface temperature of 17°C. The black vertical dashed lines represent salinities of 3 and 12. The black horizontal solid line indicates the annual mean atmospheric pCO_2 level. **(a)** and **(c)** for the *Carson* cruises cover the whole bay while inserted **(b)** and **(d)** for the *DNR* cruises only cover the upper and middle bay.

than the model-generated value (-2.7 ± 9.0 mmol m⁻² d⁻¹) in Shen et al. (2019), indicating potential interannual variability which is related to a dry hydrological condition in 2015–2017 and a wet hydrological condition in 2018 and 2019 (*see* "Discussion" section). To get a representative annual CO_2 flux in 2016, we incorporated the model-generated lower bay CO_2 fluxes in the spring and winter. As for the data gap in the upper and middle bay in January and February, the December value was used for January and the March value for February according to similar Susquehanna River discharge (Table 1).

The upper bay was a strong source of CO_2 to the atmosphere throughout the year (31.2 ± 5.6 mmol m⁻² d⁻¹), except that it was in equilibrium with the atmosphere in December (Table 2). The release of CO_2 to the atmosphere was pronounced in March (67.0 ± 34.4 mmol m⁻² d⁻¹) and in September (92.4 ± 40.9 mmol m⁻² d⁻¹). The middle bay was a CO_2 sink (-5.8 ± 1.3 mmol m⁻² d⁻¹) and the lower bay was in a balanced condition (1.0 ± 1.6 mmol m⁻² d⁻¹), which are significantly smaller than in the upper bay. Area-integrated air–water CO_2 flux estimate suggests that the whole bay was a

Table 2. Mean ± SD of monthly, seasonal, and annual area-weighted air–water CO_2 fluxes (mmol C m^{-2} d^{-1}) and annual fluxes (mol C). A positive number means water is releasing CO_2 gas to the atmosphere.

| | | CO_2 flux (mmol C m^{-2} d^{-1}) | | | | CO_2 flux (×10^9 mol C) | | | |
| | | Upper bay 5.96 × 10^8 | Middle bay 1.87 × 10^9 | Lower bay 2.74 × 10^9 | Whole bay 5.21 × 10^9 | Upper bay 5.96 × 10^8 | Middle bay 1.87 × 10^9 | Lower bay 2.74 × 10^9 | Whole bay 5.21 × 10^9 |
Season	Month								
Spring	2016-03	67.0 ± 34.4	−18.9 ± 6.7	−1.5 ± 5.3*	0.1 ± 9.1	1.2 ± 0.6	−1.1 ± 0.4	−0.1 ± 0.4*	0.0 ± 1.4
	2016-04	22.9 ± 14.8	−10.4 ± 4.8	−1.5 ± 5.3*	−1.9 ± 6.2	0.4 ± 0.3	−0.6 ± 0.3	−0.1 ± 0.4*	−0.3 ± 1.0
	2016-05†	14.9 ± 2.6	−3.6 ± 0.5	−1.5 ± 5.3*	−0.4 ± 3.3	0.3 ± 0.0	−0.2 ± 0.0	−0.1 ± 0.4*	−0.1 ± 0.5
		(16.1 ± 11.3)	(−4.3 ± 1.8)		(−0.5 ± 4.7)	(0.3 ± 0.2)	(−0.2 ± 0.1)		(−0.1 ± 0.7)
	Seasonal avg†	34.9 ± 12.5	−11.0 ± 2.8	−1.5 ± 3.1	−0.7 ± 3.8	1.9 ± 0.7	−1.8 ± 0.5	−0.4 ± 0.8	−0.3 ± 1.8
		(35.3 ± 13.0)	(−11.2 ± 2.8)		(−0.8 ± 4.0)	(1.9 ± 0.7)	(−1.9 ± 0.5)		(−0.4 ± 1.9)
Summer	2016-06†	34.2 ± 5.0	2.0 ± 0.4	2.8 ± 0.4	6.1 ± 0.9	0.6 ± 0.1	0.1 ± 0.0	0.2 ± 0.0	1.0 ± 0.1
		(36.8 ± 23.5)	(1.5 ± 2.1)	(1.6 ± 1.1)	(5.6 ± 4.0)	(0.7 ± 0.4)	(0.1 ± 0.1)	(0.1 ± 0.1)	(0.9 ± 0.6)
	2016-07	29.9 ± 13.0	−6.8 ± 2.1	1.5 ± 0.2‡	1.8 ± 2.3	0.5 ± 0.2	−0.4 ± 0.1	0.1 ± 0.0‡	0.3 ± 0.4
	2016-08†	10.9 ± 3.2	1.8 ± 0.3	0.1 ± 0.2	2.0 ± 0.6	0.2 ± 0.1	0.1 ± 0.0	0.0 ± 0.0	0.3 ± 0.1
		(33.5 ± 19.8)	(5.3 ± 2.4)	(1.2 ± 0.9)	(6.4 ± 3.6)	(0.6 ± 0.4)	(0.3 ± 0.1)	(0.1 ± 0.1)	(1.0 ± 0.6)
	Seasonal avg†	25.0 ± 4.8	−1.0 ± 0.7	1.5 ± 0.2	3.3 ± 0.9	1.3 ± 0.3	−0.2 ± 0.1	0.4 ± 0.0	1.5 ± 0.4
		(33.4 ± 11.1)	(0.0 ± 1.3)	(1.4 ± 0.5)	(4.6 ± 2.0)	(1.8 ± 0.6)	(0.0 ± 0.2)	(0.4 ± 0.1)	(2.1 ± 0.9)
Fall	2016-09	92.4 ± 40.9	14.9 ± 5.2	5.3 ± 0.6‡	18.7 ± 6.8	1.7 ± 0.7	0.8 ± 0.3	0.4 ± 0.0‡	2.9 ± 1.1
	2016-10†	29.8 ± 4.4	16.0 ± 1.5	10.5 ± 1.1	14.7 ± 1.6	0.5 ± 0.1	0.9 ± 0.1	0.9 ± 0.1	2.3 ± 0.3
		(28.3 ± 15.9)	(13.8 ± 4.9)	(11.2 ± 3.9)	(14.1 ± 5.7)	(0.5 ± 0.3)	(0.8 ± 0.3)	(0.9 ± 0.3)	(2.2 ± 0.9)
	2016-11	6.5 ± 5.7	−13.3 ± 6.7	3.9 ± 4.5‡	−2.0 ± 5.5	0.1 ± 0.1	−0.7 ± 0.4	0.3 ± 0.4‡	−0.3 ± 0.9
	Seasonal avg†	42.9 ± 13.8	5.9 ± 2.9	6.6 ± 1.6	10.5 ± 3.0	2.3 ± 0.7	1.0 ± 0.5	1.6 ± 0.4	4.9 ± 1.4
		(42.4 ± 14.8)	(5.1 ± 3.3)	(7.2 ± 2.2)	(10.5 ± 3.7)	(2.3 ± 0.8)	(0.9 ± 0.5)	(1.8 ± 0.5)	(4.9 ± 1.7)
Winter	2016-12	−0.4 ± 3.9	−16.2 ± 4.7	−2.7 ± 9.0*	−7.3 ± 6.9	0.0 ± 0.1	−0.9 ± 0.3	−0.2 ± 0.7*	−1.1 ± 1.1
	2016-01	−0.4 ± 3.9*	−16.2 ± 4.7*	−2.7 ± 9.0*	−7.3 ± 6.9	0.0 ± 0.1*	−0.9 ± 0.3*	−0.2 ± 0.7*	−1.1 ± 1.1
	2016-02	67.0 ± 34.4*	−18.9 ± 6.7*	−2.7 ± 9.0*	−0.5 ± 11.1	1.2 ± 0.6*	−1.1 ± 0.4*	−0.2 ± 0.7*	−0.1 ± 1.7
	Seasonal avg	22.1 ± 11.6	−17.1 ± 3.2	−2.7 ± 5.2	−5.0 ± 4.9	1.2 ± 0.6	−2.9 ± 0.5	−0.7 ± 1.3	−2.4 ± 2.3
Annual		31.2 ± 5.6	−5.8 ± 1.3	1.0 ± 1.6	2.0 ± 1.7	6.7 ± 1.2	−3.9 ± 0.9	0.9 ± 1.5	3.7 ± 3.3
		(33.3 ± 6.4)	(−5.8 ± 1.4)	(1.1 ± 1.6)	(2.3 ± 1.9)	(7.1 ± 1.4)	(−3.9 ± 0.9)	(1.1 ± 1.6)	(4.3 ± 3.6)
2019-02†		15.5 ± 2.5	−14.6 ± 1.4	−14.2 ± 1.5	−10.9 ± 1.6	0.3 ± 0.0	−0.8 ± 0.1	−1.2 ± 0.1	−1.7 ± 0.2
		(25.2 ± 9.6)	(−16.4 ± 4.4)	(−15.9 ± 3.9)	(−11.4 ± 4.7)	(0.5 ± 0.2)	(−0.9 ± 0.2)	(−1.3 ± 0.3)	(−1.8 ± 0.7)

*Months when field work was not conducted. Model-generated CO_2 fluxes are used to represent the missing CO_2 fluxes in the lower bay during spring and winter. For the upper and middle bay in January and February, the December value was used for January and the March value for February according to similar Susquehanna River discharge.

†Underway measurements and discrete samples calculated CO_2 flux are reported with discrete data in parentheses.

‡Months when field work was not conducted in the subsection. CO_2 flux is estimated by linearly regressing data from the months before and after.

weak CO$_2$ source (2.0 ± 1.7 mmol m^{-2} d^{-1}) with area-weighted annual CO$_2$ flux of $3.7 \pm 3.3 \times 10^9$ mol in 2016. By comparison, if we replace the February CO$_2$ flux in the current estimate with our February 2019 field observations, the annual CO$_2$ flux (-0.3×10^9 mol) tends to be nearly balanced.

Discussion

Controlling mechanisms of spatial and temporal variations in surface pCO$_2$

Regional dominance of biological production and respiration

Estuaries are characterized by a large range of pCO$_2$ which is related to net CO$_2$ inputs from external and internal sources, seasonal temperature change, air–water gas exchange, and the metabolic state of the system. To explain biological modulation of surface pCO$_2$, field observations of pCO$_2$% and DO% are shown in Fig. 5 with each plot being divided into four quadrants. Quadrants I and III represent heating and cooling, respectively. Quadrants II and IV indicate biological respiration and production, respectively. Here, we focus on comparing production and respiration.

Net respiration and production determine the regional and seasonal characteristics and levels of surface pCO$_2$ (Figs. 3, 5). High biological respiration sustains the oversaturated pCO$_2$ in the upper bay demonstrated by undersaturated DO (quadrant II) from May to October. Notably, respiration was the only dominant

metabolic state in May and October, while production was also observed in June and August. Moderate net respiration and production sustain the oversaturated and undersaturated pCO$_2$ in the upper-reach and lower-reach of the middle bay, respectively, from May to August. The boundary between the two subsections is near 38.5°N (Fig. 3), or at a surface salinity of about 12 (Fig. 4). However, net respiration dominantly determines the middle bay oversaturated pCO$_2$ in September and October. The lower bay had a nearly balanced metabolism, resulting in surface pCO$_2$ in nearly equilibrium with respect to the atmosphere. One exception is that a hurricane triggered bloom in October rapidly increased surface DO% and drove the middle and lower bays to be autotrophic in 2–3 d. Overall, high turbidity in estuaries limits gross primary production even if there are large amounts of nutrients (Gattuso et al. 1998), sustaining the oversaturated pCO$_2$ in the upper and middle bay. In contrast, low turbidity, as well as favorable temperature and riverine nutrient input, result in high production and undersaturated surface pCO$_2$ in the lower-reach of the upper bay and middle bay.

Seasonal temperature change and air–water gas exchange also contribute to surface pCO$_2$ variations, while these processes are usually overwhelmed by metabolic balance in productive estuaries. For example. in the upper bay, an increase in temperature increases pCO$_2$% and DO% due to thermodynamic effects from May to August, which could explain the pCO$_2$% increase but not the decreasing DO%. Respiration
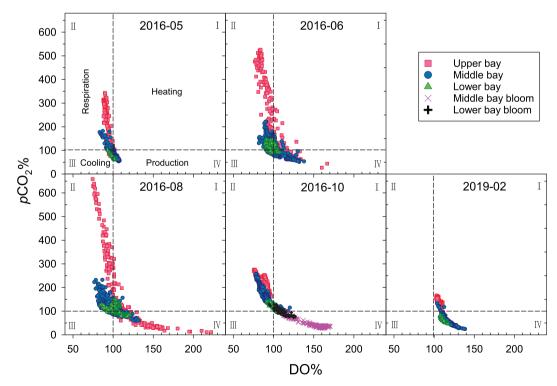

Fig. 5. Relationship of percent saturation of pCO$_2$ (pCO$_2$%) and DO (DO%) in surface waters of the upper, middle, and lower bay, respectively, observed in 2016 and 2019. The vertical and horizontal black, dashed lines represent 100% pCO$_2$ and 100% DO references. Quadrants I and III represent heating and cooling, respectively. Quadrants II and IV indicate biological respiration and production, respectively.

rapidly decreases DO% and sustains the undersaturated DO%. Gas exchange also rapidly degasses CO_2 into the atmosphere as shown by 100% DO and > 100% $p CO_2$ in June and August. For a water mass with 2500 μatm $p CO_2$, the surface water needs ~ 60 d to degas to be in equilibrium with the atmosphere. Since the bay has a 180 d average water residence time, ventilation of CO_2 to the atmosphere allows the water in the middle and lower bay to be equilibrated with the atmosphere and further can allow biological production to drive the surface to be a CO_2 sink.

There is a limitation involved in interpreting the relationship of $p CO_2$% and DO%. This analysis assumes equilibrium between water and air with 100% DO and $p CO_2$ as a reference. For the winter data in the Chesapeake Bay, surface $p CO_2$ was consistently lower than the atmosphere due to the low surface temperature. The reference point for metabolic balance should be < 100% $p CO_2$ while ~ 100% DO due to fast air–water gas exchange rate for oxygen. High gas exchange rates and low primary production in winter sustained nearly saturated DO, even if $p CO_2$% was oversaturated. Although bubble injection increasing DO% can be neglected when wind speed is lower than 10 m s^{-1} (Emerson et al. 2019), sustained wind gusts higher than this value were observed intermittently, which could partially contribute to oversaturated DO% in surface waters. Besides, the supersaturated DO% in February was majorly controlled by high biological production.

Influence of river-borne CO_2 input on regulating surface pCO_2 in the estuary

River-borne high $p CO_2$ is a product of the microbial degradation of organic matter in river water, sediments, and soils,

which can be an important process sustaining high estuarine $p CO_2$ (Borges et al. 2006). We use riverine excess DIC ($DIC_{Excess-R}$) proposed by Abril et al. (2000) to evaluate the seasonal patterns and magnitude of river-borne CO_2. It is calculated as the difference between the in situ DIC ($DIC_{Measured}$) and DIC calculated from atmospheric $p CO_2$ and in situ total alkalinity (TA) at in situ temperature and salinity (DIC_{Equil}), see Eq. 5. Here we calculate TA from DIC and pH to avoid the potential influence of organic alkalinity.

$$DIC_{Excess-R} = DIC_{Measured} - DIC_{Equil} \qquad (5)$$

The $DIC_{Excess-R}$ concentrations were all positive and controlled by both river discharge and the seasonal temperature cycle (Fig. 6). $DIC_{Excess-R}$ covaries with Riverine $p CO_2$, indicating that the Susquehanna River exports $DIC_{Excess-R}$ into the bay and contributes dynamically to monthly surface $p CO_2$ levels within the bay. $DIC_{Excess-R}$ were high in February and March (up to 155 μmol kg^{-1}) when discharge was high and temperature was low, and in June and July (up to 156 μmol kg^{-1}) when discharge was low and temperature was high. A high discharge rapidly flushes large amounts of respired products, and therefore corresponds to high $DIC_{Excess-R}$ and observed oversaturated $p CO_2$ in the upper bay (Fig. 3). River discharge peaked in February, while the $DIC_{Excess-R}$ was smaller than in March. It was because the end-member was sampled on 01 February during which daily discharge was one-third of the monthly mean value in February and a half that of March. Scaling up the $p CO_2$ in February by discharge results in higher $DIC_{Excess-R}$ in February. Although discharge was low in June and July, the high temperature supported
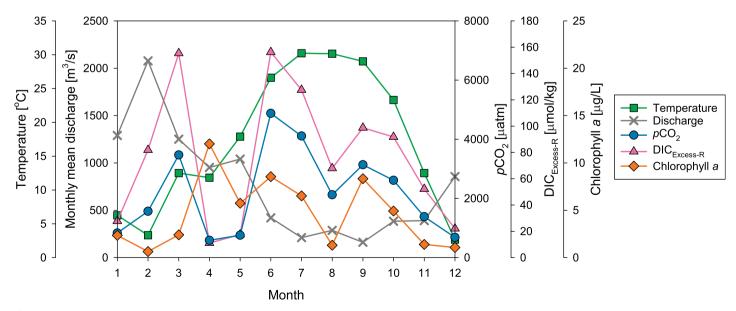

Fig. 6. Monthly mean surface temperature, discharge, surface $p CO_2$, and $DIC_{Excess-R}$ of the Susquehanna River in 2016. Monthly mean Susquehanna River discharge is from USGS site #01578310. Monthly mean Chlorophyll *a* was measurements at the Susquehanna River mouth (Sta. CB1.0) of the Chesapeake Bay Program.

microbial respiration in the river, increasing $DIC_{Excess-R}$ and supporting oversaturated pCO$_2$ downstream. The lowest $DIC_{Excess-R}$ was observed in April and May (as low as 11 μmol kg^{-1}) which is explained by the spring blooms in the river and supported by the highest Chl a. Nutrients flushed downstream in February and March also triggered spring bloom and undersaturated pCO$_2$ in the upper-reach of the upper bay in April and May (Fig. 3). Moderate $DIC_{Excess-R}$ from June to October also sustained high surface pCO$_2$ in the upper bay. One exception was in August (68 μmol kg^{-1}) which was lower than months before and after, indicating utilization of inorganic nutrients and carbon in the reservoir right above a dam in the Susquehanna River, which was not reflected by the low Chl a downstream of the dam due to low river discharge. Additionally, very low $DIC_{Excess-R}$ observed in winter (as low as 22 μmol kg^{-1}) can be attributed to low temperature and organic matter respiration rates. In summary, positive values of $DIC_{Excess-R}$ suggest the importance of river-borne CO$_2$ in sustaining oversaturated pCO$_2$ in the upper bay.

Rivers in the middle and lower bay, including the Rappahannock, James, and Potomac Rivers, are also supersaturated with CO$_2$ (Raymond et al. 2000). However, they have much smaller discharges than the Susquehanna River, so they are unlikely to have pronounced effect on pCO$_2$ as the Susquehanna River. Previous studies have found that the James River had little impact on main stem chemistry (Wong 1979; Fisher et al. 1988) and that the others may be the same because most of the river constituents are processed in the sub-estuary (Boynton et al. 1995). So, it is likely that river-borne CO$_2$ is not as significant in the middle and lower bay as it is in the upper bay, as demonstrated by that the middle bay is characterized by moderate respiration in the upper portion and moderate production in the lower portion.

Influence of excess DIC from within an estuary on regulating surface pCO₂

To measure a net addition or removal of DIC within an estuary, net excess DIC ($DIC_{Excess-net}$) within the bay is estimated by the difference between excess DIC at each station ($DIC_{Excess-B}$, same calculation as $DIC_{Excess-R}$) and mixing-corrected contribution from $DIC_{Excess-R}$ ($DIC_{Excess-mixing}$) (Eq. 6 and Fig. 7). $DIC_{Excess-mixing}$ at each station is calculated from a conservative mixing between river and ocean end-members and the salinity on stations ($S_{Measured}$) (Eq. 7).

$$DIC_{Excess-net} = DIC_{Excess-B} - DIC_{Excess-mixing} \qquad (6)$$

$$DIC_{Excess-mixing} = DIC_{Excess-R} - \frac{DIC_{Excess-R} \times S_{Measured}}{31} \qquad (7)$$

Since pCO$_2$ at the bay mouth was nearly equilibrated with the atmosphere, the ocean end-member is characterized by zero $DIC_{Excess-R}$ with an average salinity of 31 (Eq. 7). Thus if

$DIC_{Excess-B}$ is 0, it means all river delivered excess DIC is degassed to the atmosphere or consumed by biological production, as shown by a negative $DIC_{Excess-net}$. And if $DIC_{Excess-B}$ equals to the mixing corrected $DIC_{Excess-R}$, it means all riverine excess is transported to the coastal ocean, as shown by a zero $DIC_{Excess-net}$. A positive $DIC_{Excess-net}$ indicates an addition of DIC to the estuary.

Large inputs of $DIC_{Excess-R}$ were observed in March, June, and July (Fig. 6), as shown by large differences between $DIC_{Excess-B}$ and $DIC_{Excess-net}$. During these months when the input of $DIC_{Excess-R}$ was at a maximum, large amounts of nutrients were also carried to the estuary, stimulating the biological consumption of DIC as shown by negative $DIC_{Excess-net}$ values as low as -200 μmol kg^{-1}. That sustained undersaturated surface pCO$_2$ in the middle bay in March and July. Although net large DIC removal was observed, surface pCO$_2$ was still supersaturated in the upper bay in all 3 months and the upper-reach of the middle bay in June, suggesting the important role of river-borne CO$_2$ in sustaining CO$_2$ degassing in this region. In contrast, $DIC_{Excess-R}$ roughly counterbalanced the DIC removal in the lower portion of the middle bay and the entire lower bay in June, resulting in surface pCO$_2$ nearly equilibrated with respect to the atmosphere.

For months with low $DIC_{Excess-R}$ input in April, May, and December, local respiration of organic matter releases CO$_2$ into the surface water to support the oversaturated pCO$_2$ in the upper bay in April and May, as indicated by a positive $DIC_{Excess-net}$ of 0–50 μmol kg^{-1}. By comparison, $DIC_{Excess-net}$ was close to 0 in the upper bay in December, indicating nearly balanced DIC addition and removal. In this case, riverine pCO$_2$ and the observed surface pCO$_2$ in the bay are on the same level. In addition, due to potentially fewer allochthonous organic matter to support respiration in the middle and lower bay resulting from large distance away from the river mouth, net DIC removal driven by biological production over respiration sustained undersaturated surface pCO$_2$.

Moderate $DIC_{Excess-R}$ was observed from August to October due to decreasing river discharge. In August, net DIC removal within the bay through biological production was the major driver of the undersaturated surface pCO$_2$ in the lower portion of the upper bay, with favorable temperature and moderate inputs of nutrients from the river. By comparison, considering low river discharge and erosion of surface stratification in fall, the net DIC addition and removal can be related to the upward mixing of CO$_2$ and nutrient rich subsurface water into the surface and subsequent biological production. The dynamic feature did not support sustained net DIC removal while supported fluctuations in $DIC_{Excess-net}$ between positive and negative values. In this case, both $DIC_{Excess-R}$ and high pCO$_2$ subsurface water supported the oversaturated surface pCO$_2$ from August to October.

Influence of variation in hydrological months on air–water CO₂ flux

The difference in CO$_2$ flux estimates of February between the field measurement in 2019 (-14.2 ± 1.5 mmol m^{-2} d^{-1})

and the model-generated value in 2016 (– 2.7 ± 9.0 mmol m^{-2} d^{-1}) indicates a potential interannual variation. Given the inputs of riverine properties affecting the biogeochemical processes within the bay are associated with river discharge, we use the Susquehanna River discharge (~ 60% of the total river discharge to the Chesapeake Bay) to identify dry and wet hydrologic months (Fig. 8a). We use the lower bay as a case study due to its relatively invariant surface pCO₂ allowing for a simple simulation. The Susquehanna River water needs 2–3 months to reach the lower bay and the water resident time

in the lower bay is about 4 months (Du and Shen 2016). We use the mean discharge from September to December in the previous year to identify the dry or wet hydrological status in the lower bay in February of the next year. Due to high discharge in these months of 2011 and 2018 (~ 2500 m^3 s^{-1}), February 2012 and 2019 are wet months. By comparison, due to low discharge from 2015 to 2017 (~ 500 m^3 s^{-1}), February 2016 and 2017 are dry months. Corresponding biogeochemical data from the Chesapeake Bay Program are used to study the difference between dry and wet months.
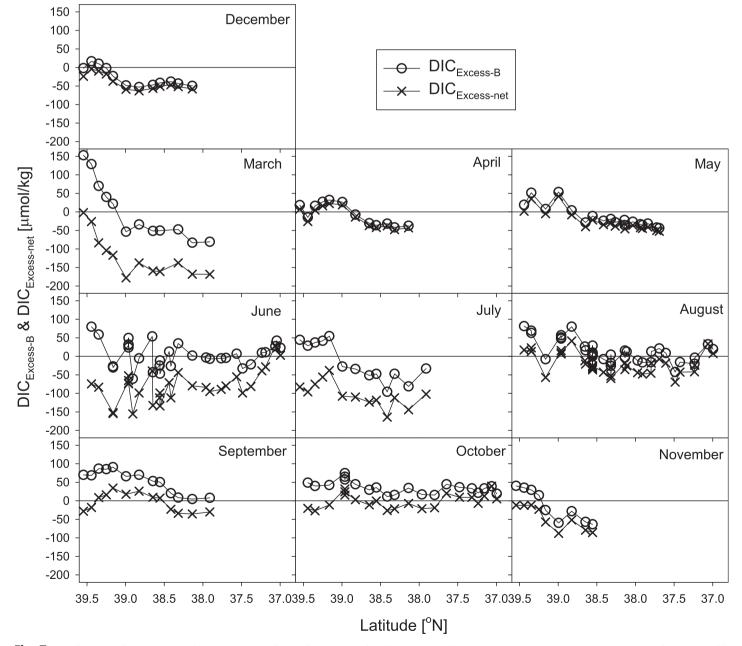

Fig. 7. Distributions of DIC$_{Excess-B}$ and DIC$_{Excess-net}$ at all sampling stations for the *Carson* and *DNR* cruises in 2016. Positive DIC$_{Excess-net}$ indicates an addition of DIC to the surface water via all estuarine internal processes and negative DIC$_{Excess-net}$ indicates a removal.
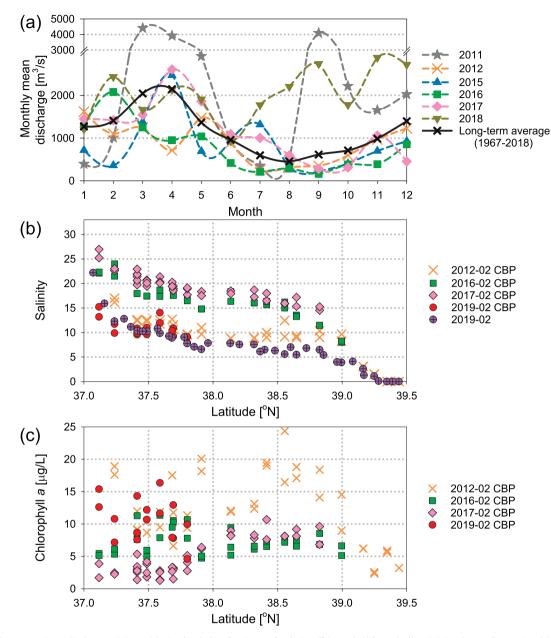
Fig. 8. Monthly mean river discharge **(a)** and latitudinal distributions of salinity **(b)** and Chlorophyll *a* **(c)** in the surface mixed layer. The long-term mean river discharge in **(a)** is an average from 1967 to 2018 reported at USGS site #01578310. The salinity and Chlorophyll *a* data from February 2012, 2016, 2017, and 2019 in **(b)** and **(c)** are from the Chesapeake Bay Program (CBP). The February 2019 salinity (purple solid crossed dot) is from the *Carson* cruise. All salinity and Chlorophyll *a* are observations in the surface mixed layer.

Same hydrological scenarios have same levels of salinity (e.g., wet February for 2012 (13.5 ± 3.0) and 2019 (11.9 ± 3.2), and dry February for 2016 (19.9 ± 2.9) and 2017 (21.4 ± 2.9)). Salinities in wet months (5 < S < 15) are systematically lower than dry months (15 < S < 25) (Fig. 8b). Correspondingly, Chl *a* in wet months (11.4 ± 3.5 for 2012 and 10.9 ± 3.1 for 2019) are distinguishable higher than dry months (7.9 ± 2.6 for 2016 and 2.9 ± 1.0 for 2017) (Fig. 8c), indicating higher biological production in wet months which increased the air–water CO₂ influx. This conclusion is

supported by the more negative CO₂ flux in February 2019 than February 2016.

We further evaluate the influence of hydrological variation on CO₂ flux by simulating how surface *p*CO₂ evolves from October to March in the lower bay and comparing the simulated values to the February 2019 observational data with the same salinity (Fig. 9). Due to the similarity in biogeochemical properties among the same type hydrological months, we use lower bay field observations in October 2016 to represent October 2015. Then the carbonate properties in October 2015
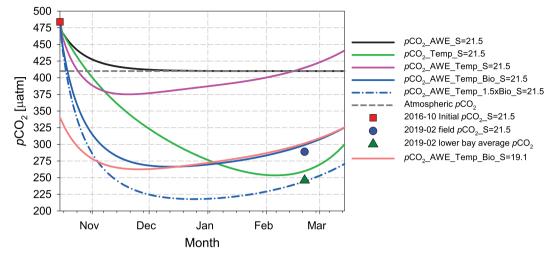
Fig. 9. Simulation of surface pCO_2 variation in the lower bay from late fall to early spring. AWE, temp, and bio denote air–water gas exchange, temperature variation, and biological activity, respectively. The red square indicates the initial pCO_2 value observed in the lower bay in October 2016 for the simulation. The blue dot shows the field pCO_2 measurement at the salinity of 21.5 at the bay mouth in February 2019. The green triangle denotes the mean pCO_2 in the lower bay in February 2019.

are used as initial inputs to simulate pCO_2 level in February 2016 (dry month), *see* details in methods. In this simulation, water pCO_2 reached equilibrium with the atmosphere (410 μatm) in December, and was unchanged thereafter when only air–water gas exchange is assumed to contribute to pCO_2 variation (solid black line). In contrast, surface pCO_2 could be lower than the field measurement (blue dot, 289 μatm) by 30 μatm when only the temperature drop explains surface pCO_2 variation (solid green line). By coupling gas exchange with temperature variation, decreasing pCO_2 caused by a fast temperature drop could be reversed by significant replenishing of CO_2 via gas exchange, showing a simulated surface pCO_2 of 414 μatm in February (solid purple line). In this sense, observed pCO_2 values were a combined effect of processes including temperature variation, air–water gas exchange, and biological production, leading to a simulated pCO_2 of 300 μatm for February 2016 (solid blue line). Additionally, we simulate pCO_2 evolvement with different initial pCO_2 and salinity values, while keeping the same DIC removal rate (solid orange vs. solid blue lines). The simulation shows nearly identical pCO_2 trends since December, indicating that the pCO_2 variation is almost independent of the initial salinity and pCO_2 values, due to the rapid interactions among physical controlling processes.

The simulated pCO_2 trend over time (solid blue line) shows high consistency with the buoy pCO_2 data at First Landing (37°N, 76.1°W, Fig. 1) from October 2018 to March 2019 (https://www.pmel.noaa.gov/co2/story/First+Landing+OA), while slightly different in magnitude due to various hydrological conditions. Lower buoy pCO_2 than simulated values support the assumption of the increased biological production in wet months. In addition, mean pCO_2 and salinity in the lower bay (green triangle, 240 ± 20 μatm, S = 16) was 49 μatm and

5.5 lower than near the bay mouth (blue dot, 289 μatm, S = 21.5) in February 2019. The latter agrees with the simulated pCO_2 (300 μatm, S = 21.5) for February 2016, indicating higher pCO_2 along with less influence from riverine inputs. The pCO_2 difference in the lower bay between simulation for February 2016 and field observation in February 2019 can be explained by using 1.5 times DIC removal rate in the simulation (dash-dotted blue line) to get a simulated surface pCO_2 of 244 μatm. In summary, in addition to wet hydrological months, CO_2 efflux in wet hydrological years might also be smaller than dry years due to overall higher nutrient input stimulated blooms, but future observations are needed to delineate the integrated differences year-round.

Uncertainties of air–water CO₂ flux estimate and future work
CO₂ flux calculation in estuarine environments

Although various algorithms have been generated to calculate air–water CO_2 flux, it should be noted that there is no satisfactory algorithm to quantify gas transfer velocity in estuaries because (1) complex turbulence at the air–water interface, which is affected by the variability in water depth, tidal current, and bottom stress (Raymond and Cole 2001; Zappa et al. 2007); and (2) the fact that gas transfer velocities have not been widely measured in estuaries. The algorithm developed by Wanninkhof (2014), used in this study, produces good estimates within a wind speed range of 3–15 m s^{-1}, a range that covers conditions in the Chesapeake Bay. The Chesapeake Bay has a large surface area and is a microtidal system, so the selected algorithm works well in most sites on the bay. However, future work is still needed to validate the best gas transfer velocity in large estuaries and bay systems.

Diel variation

CO_2 diel fluctuations vary significantly in various environments with large variations in estuaries (Dai et al. 2009). To get a representative CO_2 flux estimate, we conducted repeated transects over the same region at various times to reduce the uncertainty of the estimated CO_2 flux attributed to the snapshot underway approach. Since we surveyed the same subregion of the Chesapeake Bay in the same day, mean pCO_2 difference between repeated transects within the same subregion is a measure of the performance of this approach. The smaller the difference, the better coverage of the diel cycle. The upper bay had the largest mean of 199 μatm and the lower and middle bay had small mean values of 16 and 18 μatm, respectively. Although it only results in small uncertainties in CO_2 flux estimate of 0.5, 0.1, and 0.2 mmol m^{-2} d^{-1} for the upper, middle, and lower bay, respectively, the relatively larger difference in the dynamic upper bay reflects the need for introducing high frequency underway monitoring or mooring observations.

Spatial gradient from the main stem to nearshore

We assumed that there are no lateral variations in pCO_2 in the main stem. To verify it, we conducted transects to enter the Choptank River in June and August 2016 and the Potomac River in August 2016 to study the pCO_2 gradient. Surface pCO_2 showed small fluctuations ($\pm$ 10 μatm) from the main stem to the Choptank and Potomac River mouth while increased rapidly when entering the rivers. Over the areas we surveyed, surface pCO_2 increased by 70 μatm in the Potomac River, and by 158 μatm in June and 305 μatm in August in the Choptank River. Although the lateral gradients in the main stem are not significant, it should be noted that the actual difference might be larger under the influence of northerly and southerly winds, which drive upwelling of CO_2-rich subsurface water into the surface in nearshore areas via Ekman transport (Huang et al. 2019). However, this large signal is not included in the CO_2 flux estimate of the main stem, and future work is needed to get a complete, more accurate estimate.

Low-resolution discrete vs. high-resolution underway pCO₂ measurements

We used underway measurements of pCO_2 and calculated pCO_2 to get high spatiotemporal coverage of pCO_2. Although using calculated or measured pCO_2 has small differences in the estimated CO_2 flux, another uncertainty in the CO_2 flux estimate comes from sampling resolution, particularly for sampling patchy blooms located in between the sampling stations for the discrete measurements. For example, CO_2 flux is 10.9 $\pm$ 3.2 mmol C m^{-2} d^{-1} for underway measurement and 33.5 $\pm$ 19.8 mmol C m^{-2} d^{-1} for discrete samples in the upper bay in August, with the lower CO_2 flux relating to bloom sampled by underway. In this case, underway measurements had the advantage of capturing fine, undersaturated pCO_2 signals, which could result in a CO_2 flux one third of that from discrete data in bloom seasons. Generally, using a combination of evenly distributed and dense sampling sites can successfully reduce the uncertainties in CO_2 flux estimate.

A comparison of CO₂ flux estimates from various approaches

The estimated CO_2 flux in 2016 ($3.7 \pm 3.3 \times 10^9$ mol C) in this work is more positive than a model study of $- 12 \times 10^9$ mol C (Shen et al. 2019) and a conservative mixing model and mass balance analysis of $- 5.7 \pm 8.2 \times 10^9$ mol C (Brodeur et al. 2019), while comparable with a field study of $- 1.8 \times 10^9$ mol C for the middle and lower bay (Friedman et al. 2020). In contrast, if our February 2019 data is incorporated into the CO_2 flux estimate for 2016, the delivered annual flux would be $- 0.3 \times 10^9$ mol C. Large variations in estimated CO_2 flux indicate that further work is needed to constrain the uncertainty residing in various estimation approaches and when incorporating multi-year observations.

Shen et al. (2019) only used our spring to fall *Carson* cruises data for validation and reproduced similar trend of seasonal variation in CO_2 flux, although highly variable with oscillations between CO_2 release and uptake in the middle and lower bay were observed. The difference in CO_2 flux between the model study and this study might be caused by the lack of data for validation, particularly for the high discharge months (such as *DNR* and winter *Carson* cruises), to optimize the model. For example, the model results had smaller pCO_2 in the river mouth and larger biological production in the upper and middle bay than the field observations. On the other hand, the difference might be related to that the model explicitly captures the lateral variations and diel cycle. Therefore, more extensive observations are needed to capture the dynamic spatial and temporal features.

Brodeur et al. (2019) estimated the carbon flux by calculating the difference in DIC inventory between input through river and export out of the bay. It should be noted that the DIC conservative mixing model used the DIC concentration of Susquehanna River to represent all rivers. Therefore, the discrepancy in CO_2 flux might be related to other DIC inputs, including other rivers, groundwater, or lateral transport. At the mouth of Potomac River, our field data showed that DIC was higher than the value predicted from the mixing line between Susquehanna River and oceanic water. It could result in a larger DIC input from rivers if we include the Potomac River, leading to a smaller difference in CO_2 flux between both studies. Therefore, extensive future work to monitor the river end-member might be important.

Friedman et al. (2020) estimated CO_2 flux in the middle and lower bay through calculated pCO_2 from discrete DIC and TA samples which were collected from four cruises spanning from November 2016 to July 2017. This study reported that the Chesapeake Bay main stem was a CO_2 sink. According to our study, the upper bay is a strong CO_2 source to the

atmosphere and should not be neglected in the CO_2 flux estimate over the bay. However, excluding the CO_2 flux in the upper bay, the annual CO_2 flux of -3.0×10^9 mol C from our study is similar to Friedman et al. (2020). Given 2016 and 2017 are classified as the same hydrological status with similar annual mean river discharge, the difference in CO_2 flux might be related to sampling frequency and resolution. In addition, the pCO_2 calculated using DIC and TA and CO2SYS is lower than measured pCO_2 due to the influence of organic alkalinity. In this case, the CO_2 flux in Friedman et al. (2020) should be more positive and shows to be a CO_2 source when including the CO_2 flux of the upper bay in our study. In summary, there is a need to reduce the uncertainty in CO_2 flux estimate using various approaches. Additionally, measurements of pCO_2 distribution in wet years is critical to understanding the interannual variation of CO_2 flux.

Summary and concluding remarks

Through high spatial and temporal coverage of pCO_2 measurements in the main stem of the Chesapeake Bay from March to December 2016 and in February 2019, we conclude that the Chesapeake Bay was a weak source of CO_2 to the atmosphere with an annual flux of $3.7 \pm 3.3 \times 10^9$ mol C for the dry hydrologic year of 2016. Chesapeake Bay is an exceptionally large estuarine system with strong spatial gradients. The upper bay was river-dominated, and a net CO_2 source throughout the year (31.2 ± 5.6 mmol C m^{-2} d^{-1}). The middle bay was a transition zone, with CO_2 degassing in the upper portion and CO_2 uptake in the lower portion. Overall, the middle bay was a CO_2 sink (-5.8 ± 1.3 mmol C m^{-2} d^{-1}). The lower bay was ocean-dominated, and showed a balanced condition (1.0 ± 1.6 mmol C m^{-2} d^{-1}). However, during wet months (such as February 2019), the lower bay was a strong CO_2 sink which will lead to a weaker bay-wide efflux or turn the bay into a CO_2 sink.

Temperature variation, air–water gas exchange, biological production/respiration, and mixing controlled surface pCO_2 distribution from the upper to the lower bay. At the subsection level, river-borne CO_2 and the respiration of allochthonous and locally produced organic carbon supported oversaturated pCO_2 in the upper bay. Because of the long water residence time, CO_2 removal from the surface water under multiple processes decreased pCO_2 from the upper bay to the middle bay to the level of atmospheric CO_2. In the lower bay, temperature variation, biological activity, and air–water gas exchange controlled the pCO_2 variation. Through this work, we reported the first comprehensive annual observation of surface pCO_2 and air–water CO_2 flux along the main stem of the Chesapeake Bay.

The interannual variability of CO_2 flux is expected to be related to variations in river flow, which controls the inputs of nutrients and organic matter into estuaries and subsequent changes in carbon cycling dynamics. To get a more complete understanding of CO_2 flux in the Chesapeake Bay, field measurements for wet months and years and interannual modeling studies could be very important to elucidate systematic controlling mechanisms. In the future, continuous field measurements of pCO_2 are also needed to capture dynamic features, to study the long-term trends of CO_2 fluxes responding to rapid climate change, and to quantify anthropogenic stresses. Yet, as we have demonstrated in this paper, a great deal of information about CO_2 flux in a large bay system with stratification, long water residence times, and extensive ocean influence can be learned. In contrast to small and medium size river-dominated estuaries which release a large amount of CO_2 to the atmosphere, the large Chesapeake Bay serves as a weak source of CO_2 with a broad spatial and temporal variation. Further studies in large bays and estuaries will be important to constrain the estimate of global carbon budget in estuaries.

References

Abril, G., H. Etcheber, A. V. Borges, and M. Frankignoulle. 2000. Excess atmospheric carbon dioxide transported by rivers into the Scheldt estuary. C. R. Acad. Sci.-Ser. IIA-Earth Planet. Sci. **330**: 761–768. doi:10.1016/s1251-8050(00)00231-7

Battin, T. J., L. A. Kaplan, S. Findlay, C. S. Hopkinson, E. Marti, A. I. Packman, J. D. Newbold, and F. Sabater. 2008. Biophysical controls on organic carbon fluxes in fluvial networks. Nat. Geosci. **1**: 95–100. doi:10.1038/ngeo101

Boesch, D. F., R. B. Brinsfield, and R. E. Magnien. 2001. Chesapeake Bay eutrophication: Scientific understanding, ecosystem restoration, and challenges for agriculture. J. Environ. Qual. **30**: 303–320. doi:10.2134/jeq2001.302303x

Borges, A. V. 2005. Do we have enough pieces of the jigsaw to integrate CO_2 fluxes in the coastal ocean? Estuaries **28**: 3–27. doi:10.1007/bf02732750

Borges, A. V., L.-S. Schiettecatte, G. Abril, B. Delille, and F. Gazeau. 2006. Carbon dioxide in European coastal waters. Estuar. Coast. Shelf Sci. **70**: 375–387. doi:10.1016/j.ecss.2006.05.046

Boynton, W. R., J. H. Garber, R. Summers, and W. M. Kemp. 1995. Inputs, transformations, and transport of nitrogen and phosphorus in Chesapeake Bay and selected tributaries. Estuaries **18**: 285–314. doi:10.2307/1352640

Boynton, W. R., and others. 1997. Interactions between physics and biology in the estuarine turbidity maximum (ETM) of Chesapeake Bay, USA. Int. Counc. Explor. Sea. *CM 1997/S*(11), Session S.

Brodeur, J. R., and others. 2019. Chesapeake Bay inorganic carbon: Spatial distribution and seasonal variability. Frontiers Mar. Sci. **6**: 99. doi:10.3389/fmars.2019.00099

Caffrey, J. M. 2004. Factors controlling net ecosystem metabolism in U.S. estuaries. Estuaries **27**: 90–101. doi:10.1007/bf02803563

Cai, W.-J. 2011. Estuarine and coastal ocean carbon paradox: CO_2 sinks or sites of terrestrial carbon incineration? Ann. Rev. Mar. Sci. **3**: 123–145. doi:10.1146/annurev-marine-120709-142723

Cai, W.-J., Y. C. Wang, and R. E. Hodson. 1998. Acid-base properties of dissolved organic matter in the estuarine waters of Georgia, USA. Geochim. Cosmochim. Acta **62**: 473–483. doi:10.1016/s0016-7037(97)00363-3

Cai, W.-J., and others. 2017. Redox reactions and weak buffering capacity lead to acidification in the Chesapeake Bay. Nat. Commun. **8**: 369. doi:10.1038/s41467-017-00417-7

Cerco, C. F., and T. Cole. 1993. Three-dimensional eutrophication model of Chesapeake Bay. J. Environ. Eng. **119**: 1006–1025. doi:10.1061/(asce)0733-9372(1993)119:6(1006)

Chen, C.-T. A., and A. V. Borges. 2009. Reconciling opposing views on carbon cycling in the coastal ocean: Continental shelves as sinks and near-shore ecosystems as sources of atmospheric CO_2. Deep-Sea Res. Part II **56**: 578–590. doi:10.1016/j.dsr2.2009.01.001

Chen, C.-T. A., T.-H. Huang, Y.-C. Chen, Y. Bai, X. He, and Y. Kang. 2013. Air-sea exchanges of CO_2 in the world's coastal seas. Biogeosciences **10**: 6509–6544. doi:10.5194/bg-10-6509-2013

Cooley, S. R., V. J. Coles, A. Subramaniam, and P. L. Yager. 2007. Seasonal variations in the Amazon plume-related atmospheric carbon sink. Global Biogeochem. Cycles **21**: GB3014. doi:10.1029/2006gb002831

Dai, M., Z. Lu, W. Zhai, B. Chen, Z. Cao, K. Zhou, W.-J. Cai, and C.-T. A. Chen. 2009. Diurnal variations of surface seawater pCO_2 in contrasting coastal environments. Limnol. Oceanogr. **54**: 735–745. doi:10.4319/lo.2009.54.3.0735

Dickson, A. G. 1990. Standard potential of the reaction: AgCl(s) +1/2H₂(g)=Ag(s)+HCl(aq), and and the standard acidity constant of the ion HSO4⁻ in synthetic sea water from 273.15 to 318.15 K. J. Chem. Thermodyn. **22**: 113–127. doi:10.1016/0021-9614(90)90074-z

Dinauer, A., and A. Mucci. 2017. Spatial variability in surface-water pCO_2 and gas exchange in the world's largest semi-enclosed estuarine system: St. Lawrence estuary (Canada). Biogeosciences **14**: 3221–3237. doi:10.5194/bg-14-3221-2017

Du, J., and J. Shen. 2016. Water residence time in Chesapeake Bay for 1980-2012. J. Mar. Syst. **164**: 101–111. doi:10.1016/j.jmarsys.2016.08.011

Emerson, S., B. Yang, M. White, and M. Cronin. 2019. Air-sea gas transfer: Determining bubble fluxes with in situ N_2 observations. J. Geophys. Res.: Oceans **124**: 2716–2727. doi:10.1029/2018jc014786

Fisher, T. R., L. W. Harding, D. W. Stanley, and L. G. Ward. 1988. Phytoplankton, nutrients, and turbidity in the Chesapeake, Delaware, and Hudson estuaries. Estuar. Coast. Shelf Sci. **27**: 61–93. doi:10.1016/0272-7714(88)90032-7

Friedman, J. R., E. H. Shadwick, M. A. M. Friedrichs, R. G. Najjar, O. A. De Meo, F. Da, and J. L. Smith. 2020. Seasonal variability of the CO_2 system in a large coastal plain estuary. J. Geophys. Res.: Oceans **125**: e2019JC015609. doi:10.1029/2019jc015609

Gattuso, J.-P., M. Frankignoulle, and R. Wollast. 1998. Carbon and carbonate metabolism in coastal aquatic ecosystems. Annu. Rev. Ecol. Syst. **29**: 405–434. 10.1146/annurev.ecolsys.29.1.405

Hagy, J. D., W. R. Boynton, C. W. Keefe, and K. V. Wood. 2004. Hypoxia in Chesapeake Bay, 1950–2001: Long-term change in relation to nutrient loading and river flow. Estuaries **27**: 634–658. doi:10.1007/bf02907650

Huang, W.-J., W.-J. Cai, Y. Wang, S. E. Lohrenz, and M. C. Murrell. 2015. The carbon dioxide system on the Mississippi River-dominated continental shelf in the northern Gulf of Mexico: 1. Distribution and air-sea CO_2 flux. J. Geophys. Res.: Oceans **120**: 1429–1445. doi:10.1002/2014jc010498

Huang, W.-J., W.-J. Cai, X. Xie, and M. Li. 2019. Wind-driven lateral variations of partial pressure of carbon dioxide in a large estuary. J. Mar. Syst. **195**: 67–73. doi:10.1016/j.jmarsys.2019.03.002

Joesoef, A., W.-J. Huang, Y. Gao, and W.-J. Cai. 2015. Air–water fluxes and sources of carbon dioxide in the Delaware estuary: Spatial and seasonal variability. Biogeosciences **12**: 6085–6101. doi:10.5194/bg-12-6085-2015

Kemp, W. M., E. M. Smith, M. MarvinDiPasquale, and W. R. Boynton. 1997. Organic carbon balance and net ecosystem metabolism in Chesapeake Bay. Mar. Ecol. Prog. Ser. **150**: 229–248. doi:10.3354/meps150229

Kemp, W. M., and others. 2005. Eutrophication of Chesapeake Bay: Historical trends and ecological interactions. Mar. Ecol. Prog. Ser. **303**: 1–29. doi:10.3354/meps303001

Kone, Y. J. M., G. Abril, K. N. Kouadio, B. Delille, and A. V. Borges. 2009. Seasonal variability of carbon dioxide in the rivers and lagoons of Ivory Coast (West Africa). Estuaries Coasts **32**: 246–260. doi:10.1007/s12237-008-9121-0

Laruelle, G. G., R. Lauerwald, J. Rotschi, P. A. Raymond, J. Hartmann, and P. Regnier. 2015. Seasonal response of air-water CO_2 exchange along the land-ocean aquatic continuum of the northeast North American coast. Biogeosciences **12**: 1447–1458. doi:10.5194/bg-12-1447-2015

Millero, F. J., T. B. Graham, F. Huang, H. Bustos-Serrano, and D. Pierrot. 2006. Dissociation constants of carbonic acid in seawater as a function of salinity and temperature. Mar. Chem. **100**: 80–94. doi:10.1016/j.marchem.2005.12.001

Officer, C. B., R. B. Biggs, J. L. Taft, L. E. Cronin, M. A. Tyler, and W. R. Boynton. 1984. Chesapeake Bay anoxia: Origin, development, and significance. Science **223**: 22–27. doi:10.1126/science.223.4631.22

Orr, J. C., J.-M. Epitalon, and J.-P. Gattuso. 2015. Comparison of ten packages that compute ocean carbonate chemistry. Biogeosciences **12**: 1483–1510. doi:10.5194/bg-12-1483-2015

Orth, R. J., and others. 2017. Submersed aquatic vegetation in Chesapeake Bay: Sentinel species in a changing world. Bioscience **67**: 698–712. doi:10.1093/biosci/bix058

Pai, S.-C., G. C. Gong, and K.-K. Liu. 1993. Determination of dissolved-oxygen in seawater by direct spectrophotometry of total iodine. Mar. Chem. **41**: 343–351. doi:10.1016/0304-4203(93)90266-q

Pierrot, D., E. Lewis, and D. W. R. Wallace. 2006. MS excel program developed for CO_2 system calculations. ORNL/CDIAC-105a. Carbon Dioxide Information Analysis Center, Oak Ridge National Laboratory, U.S. Department of Energy, Oak Ridge, Tennessee. doi: 10.3334/CDIAC/otg.CO2SYS_XLS_CDIAC105a. Available from http://cdiac.ornl.gov/ftp/co2sys/CO2SYS_calc_XLS_v2.1/.

Raymond, P. A., J. E. Bauer, and J. J. Cole. 2000. Atmospheric CO_2 evasion, dissolved inorganic carbon production, and net heterotrophy in the York River estuary. Limnol. Oceanogr. **45**: 1707–1717. doi:10.4319/lo.2000.45.8.1707

Raymond, P. A., and J. J. Cole. 2001. Gas exchange in rivers and estuaries: Choosing a gas transfer velocity. Estuaries **24**: 312–317. doi:10.2307/1352954

Shen, C., and others. 2019. Controls on carbonate system dynamics in a coastal plain estuary: A modeling study. J. Geophys. Res.: Biogeosci. **124**: 61–78. doi:10.1029/2018jg004802

Shore protection manual. 1984. Coastal Engineering Research Center, Department of the Army, Waterways Experiment Station, Vicksburg, Mississippi.

Takahashi, T., J. Olafsson, J. G. Goddard, D. W. Chipman, and S. C. Sutherland. 1993. Seasonal variation of CO_2 and nutrients in the high-latitude surface oceans: A comparative study. Global Biogeochem. Cycles **7**: 843–878. doi:10.1029/93GB02263

Uppström, L. R. 1974. The boron/chlorinity ratio of deep-sea water from the Pacific Ocean. Deep-Sea Res. Oceanogr. Abstr. **21**: 161–162. doi:10.1016/0011-7471(74)90074-6

Wanninkhof, R. 2014. Relationship between wind speed and gas exchange over the ocean revisited. Limnol. Oceanogr.: Methods **12**: 351–362. doi:10.4319/lom.2014.12.351

Wanninkhof, R., E. Lewis, R. A. Feely, and F. J. Millero. 1999. The optimal carbonate dissociation constants for determining surface water pCO_2 from alkalinity and total inorganic carbon. Mar. Chem. **65**: 291–301. doi:10.1016/s0304-4203(99)00021-3

Wong, G. T. F. 1979. Alkalinity and pH in the southern Chesapeake Bay and the James River estuary. Limnol. Oceanogr. **24**: 970–977. doi:10.4319/lo.1979.24.5.0970

Zappa, C. J., W. R. McGillis, P. A. Raymond, J. B. Edson, E. J. Hintsa, H. J. Zemmelink, J. W. H. Dacey, and D. T. Ho. 2007. Environmental turbulent mixing controls on air-water gas exchange in marine and aquatic systems. Geophys. Res. Lett. **34**: L10601. doi:10.1029/2006gl028790

Zhai, W., M. Dai, and X. Guo. 2007. Carbonate system and CO_2 degassing fluxes in the inner estuary of Changjiang (Yangtze) river, China. Mar. Chem. **107**: 342–356. doi:10.1016/j.marchem.2007.02.011

Conflict of Interest

None declared.